Brazilian Journal of Geophysics, **42** (2024), 1, 1–14
Brazilian Geophysical Society
ISSN 2764-8044
DOI 10.22564/brjg.v41i2.2299

ANISOTROPY IN STRATIFIED AND EQUIVALENT MEDIA: KINEMATIC AND AMPLITUDE ANALYSIS

Gustavo Henrique Teixeira da Silva [1*], Luiz Alberto Santos [1,2] and Marco Antonio Cetale Santos [2]

[1]Petrobras S.A., Rio de Janeiro, RJ, Brazil
[2]Universidade Federal Fluminense - UFF, Instituto de Geociências, Niterói, RJ, Brazil

*Corresponding author: gustavohts@msn.com

ABSTRACT. We implemented an elastic-anisotropic seismic modeling algorithm via synthetic models to evaluate different geological scenarios, where intercalations of sandstones and shales, carbonates and shales and halite and high-speed salt were simulated. These lithologies were selected based on their abundance in the sedimentary record and the importance they have in the composition of petroleum systems. We analyzed the results relative to kinematic and dynamic aspects to broaden the understanding of how these elements act in the presence of anisotropy. Additionally, the elastic and anisotropic parameters of intercalations composed by the referred lithologies were analytically estimated, thus obtaining the characteristics of several equivalent media. The results confirm previous postulations that the intercalation of layers with different properties can generate extrinsic anisotropy, contributing to the perspective of different wavelength(λ)/thickness ratios favorable to such effects. The results indicate that λ/thickness ratios greater than 6 are propitious for extrinsic anisotropy generation and the use of equivalent media as substitutes for stratified layers are ratified for thicknesses lower than 10 meters. Also, it was observed that in most cases, intrinsic anisotropy has a main role over extrinsic anisotropy.

Keywords: seismic anisotropy; seismic modeling; kinematic analysis; amplitude analysis; synthetic models

INTRODUCTION

Among the different steps of a seismic processing, velocity model building is critical for seismic imaging, time-depth conversion and inversion. Within this context, the variation of seismic wave velocity values as a function of the propagation angle, also known as anisotropy, appears as a prominent element, with applications especially developed from the advances made in the 1980s.

McCollum and Snell (1932) present one of the first papers where anisotropy is measured in sedimentary rocks, showing values obtained from measurements in shales. Evaluating the velocities obtained in experiments carried out parallel and orthogonally to the stratifications of the selected formation, they concluded that the propagation of waves in the horizontal direction (parallel to the bedding) presented a value 40% higher than that observed in the orthogonal direction, thus indicating the occurrence of highlighted asymmetry between the velocities for the different directions. Along the following decades, studies about the so-called long wave anisotropy seeked to evaluate the results of the propagation of relatively long-length seismic waves over layers with sub-seismic thicknesses, whose repetition in stratified media proved to be a source of relevant anisotropic effects. Within this context, Backus (1962) stands out, whose formulations allowed the magnitude estimation of the anisotropy generated by the referred lithological intercalations.

The experimental work by Melia and Carlson (1984) is one of the first efforts to understand the favorable relationships between wavelength and layer thickness for the generation of anisotropy, in addition to the influence of proportion between different materials. From physical models composed of layers of glass and epoxy, with different thicknesses and

proportions of materials, they obtained results that indicate that the highest anisotropy value was generated in the sample composed of 50% glass and 50% epoxy. They indicate too that, for wavelength versus layer thickness ratios between 10 and 100, long-wave anisotropy was generated.

One of the most important milestones in the history of anisotropic research can be referred to the article by Thomsen (1986), in which the author proposes three parameters, elaborated from combinations of elastic coefficients. From the parameters ϵ, γ and δ, Thomsen seeks to characterize the anisotropic components acting on compressional and shear waves, creating a methodology that would serve as a basis for most of the subsequent studies.

From the 1990s onwards, an increasing number of works began to investigate the consequences to seismic imaging of non-application of anisotropy. Carcione et al. (1991) is an important reference within the subject studied, presenting forward seismic modeling based on the experiments of Melia and Carlson (1984). The evaluation of wavelength ratios by layer thickness indicates that values between 6 and 8 are capable of generating the anisotropic effect related to the passage of long waves in stratified media.

The next years are rich in new researches that expand the understanding of the origin and impacts of anisotropy, especially when related to shales. Dewhurst and Siggin (2006); Singh and Sircar (2014); Okorie et al. (2016) and Aniwetalu et al. (2021) present important considerations about the magnitudes of anisotropy observed in shales, indicating that it is a lithology with characteristics conducive to the phenomenon, especially regarding the alignment of clay minerals.

Within this context, the results presented here contribute to the understanding of how anisotropy can be generated in intercalated media, where the wavelength is many times greater than the thickness of the lithological layers. From the implementation of an anisotropic elastic modeling algorithm, several scenarios are evaluated with variations in thicknesses and properties taken from different lithologies.

Additionally, the parameters of equivalent media for different geological contexts are also estimated, creating a list of highly relevant data for the understanding of how the velocity contrasts between different lithologies impact the magnitude of the generated anisotropy. Comparisons are made between the data obtained from the intecalated and equivalent media modeling, allowing the establishment of correspondences and distinctions in kinematics and amplitude terms.

The results obtained indicate that relationships between wavelength and layer thickness (λ/thickness) greater than 6 present favorable conditions for the generation of extrinsic anisotropy, formed by the intercalation of layers with different properties. The analyzes suggest too that for contexts where the considered lithologies are individually isotropic, expressive velocity contrasts between them are required so that significant anisotropies could be observed.

Also observed is that equivalent, homogeneous and anisotropic media, in different situations, can be consid-ered adequate representations of heterogeneous (stratified) media, allowing to obtain kinematically equivalent data, besides satisfactory data regarding the recorded amplitudes. Finally, it is indicated that the analysis carried out on a medium composed of isotropic sandstones and anisotropic shales reveals the outstanding importance of intrinsic anisotropy, related to the characteristic properties of the shale, especially in relation to the alignment of its mineral constituents.

MATERIALS AND METHODS

The main stages developed during the work include the estimation of the parameters of equivalent media from formulations derived from Backus (1962), as well as the anisotropic elastic seismic modeling of stratified and equivalent geological media, generating data that allow kinematic and amplitude analyses. We selected three distinct geological contexts to build the geological models, namely: dolomite and argillite intercalation, sandstone and shale intercalation and high-velocity salt and halite intercalation. The properties of these lithologies are shown in Tables 1, 2 and 3.

Regarding the association between argillites and carbonates, the reservoirs of the Albian interval of the Campos Basin can be highlighted, with emphasis on Quissamã Fm. (Lupinacci et al., 2020). The association between shales and sandstones can be observed in a large part of the sedimentary record of the basins, including in this context the turbidite deposits, responsible for large accumulations of hydrocarbons, such as in Campo de Jubarte, in Campos Basin (Teixeira, 2021). Maul et al. (2019) present important considerations about evaporite intercalations and their influence on the seismic imaging of pre-salt reservoirs.

Table 1: Dolomite and Argillite properties (Mavko et al., 2009).

Properties	Dolomite	Argillite
Vp (m/s)	5200	2900
Vs (m/s)	2700	1400
ρ (g/cm^3)	2,45	2,34
δ	0	0
ϵ	0	0
γ	0	0

Table 2: Shale and Sandstone properties (Sondergeld and Rai, 2011).

Properties	Shale	Sandstone
Vp (m/s)	3060	2950
Vs (m/s)	1490	1480
ρ (g/cm^3)	2,42	2
δ	-0,051	0
ϵ	0,256	0
γ	0,481	0

Table 3: Halite and High-Velocity Salt properties (Maul et al., 2019).

Properties	Halite	HVS
Vp (m/s)	4510	5061
Vs (m/s)	2706	3037
ρ (g/cm^3)	2,03	2,66
δ	0	0
ϵ	0	0
γ	0	0

The parameters estimated for equivalent media were calculated using the formulations as presented by Mavko et al. (2009) for cases where both lithologies are considered isotropic, while, for situations where at least one of the lithologies is anisotropic, the formulations were used as organized by Kumar (2013). For each lithological combination, we presented a graph corresponding to the anisotropic parameters estimated, where the abscissa axis represents the proportion of a given lithology in the intercalation.

For stratified media modeling, as well as the equivalent media, grids of elastic parameters (C_{11}, C_{13}, C_{33} and C_{44}) were generated, in addition to the densities (Figure 1). For the calculus of the referred stiffness matrix coefficients, the values of V_p and V_s in the vertical direction, in addition to Thomsen's parameters (ϵ and δ) were given as inputs.

The formulations used to calculate the elastic parameters are (considering just P-wave anisotropy):

$$C_{33} = V_p^2 \rho \tag{1}$$

$$C_{44} = V_s^2 \rho \tag{2}$$

$$C_{11} = C_{33}(1 + 2\epsilon) \tag{3}$$

$$C_{13} = -C_{44} + \sqrt{C_{44}^2 + C_{33}^2 + (1 + 2\delta) - C_{33}C_{44}(2 + 2\delta)} \tag{4}$$

Seeking to evaluate the impact of layers with different thicknesses on the generation of extrinsic anisotropy, we build models with thicknesses of 2.5 m, 5 m, 7.5 m, 10 m, 15 m and 20 m. These variations allow the evaluation of different relationships λ(wavelength)/layer thickness, thus indicating favorable situations for the occurrence of anisotropy in stratified media, as well as the resulting properties.

Regarding the forward seismic modeling algorithm, the general formulations used are the following, valid for VTI medium, as presented in Martins (2003):

$$\rho \frac{\delta U}{\delta t} = \frac{\delta \tau_{xx}}{\delta x} + \frac{\delta \tau_{xz}}{\delta z} \tag{5}$$

$$\rho \frac{\delta V}{\delta t} = \frac{\delta \tau_{zx}}{\delta x} + \frac{\delta \tau_{zz}}{\delta z} \tag{6}$$

$$\frac{\delta \tau_{xx}}{\delta t} = C_{11} \frac{\delta U}{\delta x} + C_{13} \frac{\delta V}{\delta z} \tag{7}$$

$$\frac{\delta \tau_{zz}}{\delta t} = C_{33} \frac{\delta V}{\delta z} + C_{13} \frac{\delta U}{\delta x} \tag{8}$$

$$\frac{\delta \tau_{zx}}{\delta t} = C_{44} \left(\frac{\delta U}{\delta z} + \frac{\delta V}{\delta x} \right) \tag{9}$$

where:

U and V: horizontal and vertical components of the velocity particle field; τ_{xx}, τ_{zz} and τ_{zx}: normal and shear tensions; and C_{mn}: elastic parameters.

The results obtained are presented in subtopics, initially divided between estimated equivalent media parameters and seismic modelings, which include the simulation of stratified lithology contexts, as well as their homogeneous equivalent media.

After the isolated presentation of these results, a comparison is made between them, seeking to analyze kinematic and dynamic (amplitudes) similarities and differences between the theoretically equivalent models. Finally, the question of extrinsic and intrinsic anisotropies is addressed, looking for indication of the influence of each of these on the general anisotropic effect.

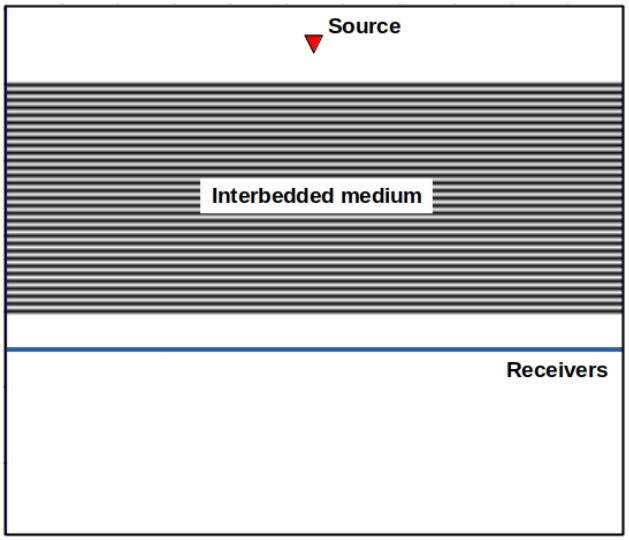

Figure 1: Example of stratified layer model.

RESULTS

Anisotropic parameters

The first results presented refer to estimates of anisotropic parameters for equivalent media with different proportions between the two lithologies that make up each of the geological contexts. Strictly speaking, as we are predominantly dealing with anisotropic media, the evaluated waves must be understood as qP and qS.

Firstly, we present the estimated effective parameters for intercalations composed by dolomite and clay (Figure 2a). The behavior of the δ parameter initially asks for attention, mainly due to its asymmetric nature. As can be seen, it presents the highest values in modulus between 60% and 70% of dolomite, with a smooth slope to the left and steeper to the right.

Contrary to the behavior observed in the δ parameter, the γ and ϵ parameters are symmetrical in their graphs, with the highest values positioned at the point relative to the proportion of 50% of each lithology. In this way, the anisotropy related to ϵ has a maximum value close to 0.17, thus configuring in the limit between the medium and strong anisotropy. The anisotropy of the qS wave (γ) reaches, at the same point, a value close to 0.27.

The effective anisotropic parameters estimated for the intercalation between shale and sandstone show a general feature of the curves different from that observed for the dolomite-argillite case, reflecting the influence of the intrinsic anisotropy of the shale. The three curves presented show a slight curvature, suggesting that the anisotropy formed by the combination of the two lithologies does not follow a strictly linear pattern (Figure 2b).

Taking for instance the point where the presence of 20% of shale in the intercalation is considered, the parameter ϵ has a value close to 0.065, thus corresponding to an anisotropy of relatively weak degree. This result allows the suggestion that even relatively small contributions of shale in a stratified medium can generate velocity-sensitive effects so that ignoring them can lead to inaccuracies in the velocity model building.

Finishing the presentation of the anisotropic parameters graphs, we show the values of an evaporitic intercalation containing halite and high-velocity salts (HVS), where these are mostly composed by anhydrite (Figure 2c). The joint occurrence of these two minerals is quite common in the Aptian evaporitic sequence of southeastern Brazilian offshore sedimentary basins.

The two lithologies are considered, individually, as isotropic so that the observed anisotropy is generated exclusively by the intercalation of the layers. The contrast of compressional velocities between the two lithotypes is relatively high, being approximately 550 m/s. This difference may be even greater due to the characteristics of anhydrite, which can have velocities up to 5500 m/s.

The parameter δ, represented by the green dashed line, has a value close to zero for the entire range of the graph, suggesting that in this context the anisotropy for the shorter offsets is not significant. As for the parameter ϵ, one of the most important anisotropic elements considered in the velocity model building, its maximum value is approximately 0.03, located at the point with equal proportions for each lithology.

Considering that the maximum estimated value for ϵ can be classified as a weak anisotropy, it can be suggested that, for halite layers with rare high-velocity salt sheets, there is no significant anisotropy and, therefore, the exclusive use of the velocity of the main lithology is sufficient for the representation. However, as previously indicated, in favorable contexts, high-velocity salts can reach P-wave velocities up to 5500 m/s, thus being able to generate a more pronounced anisotropic effect than that found in this experiment.

The intercalations evaluated for different geological contexts proved to be capable of generating and influencing the anisotropic aspects of these media, indicating that, in certain scenarios, the disregard for the alternation of layers of different properties can result in a misrepresentation and misunderstand. For cases where the two lithologies considered were isotropic, it is observed that the contrast between their parameters is a determining factor for the final anisotropy result, which is greater than the differences between the layers velocities.

For the case where we have the intrinsic anisotropy of the shale, it can be observed that the parameters δ and ϵ of this lithology strongly influence the characteristics of the equivalent medium and that laminated deposits, composed of sandstones and shales, can be inadequately represented if intercalation and its effects are not considered during the construction of the geological and velocity model.

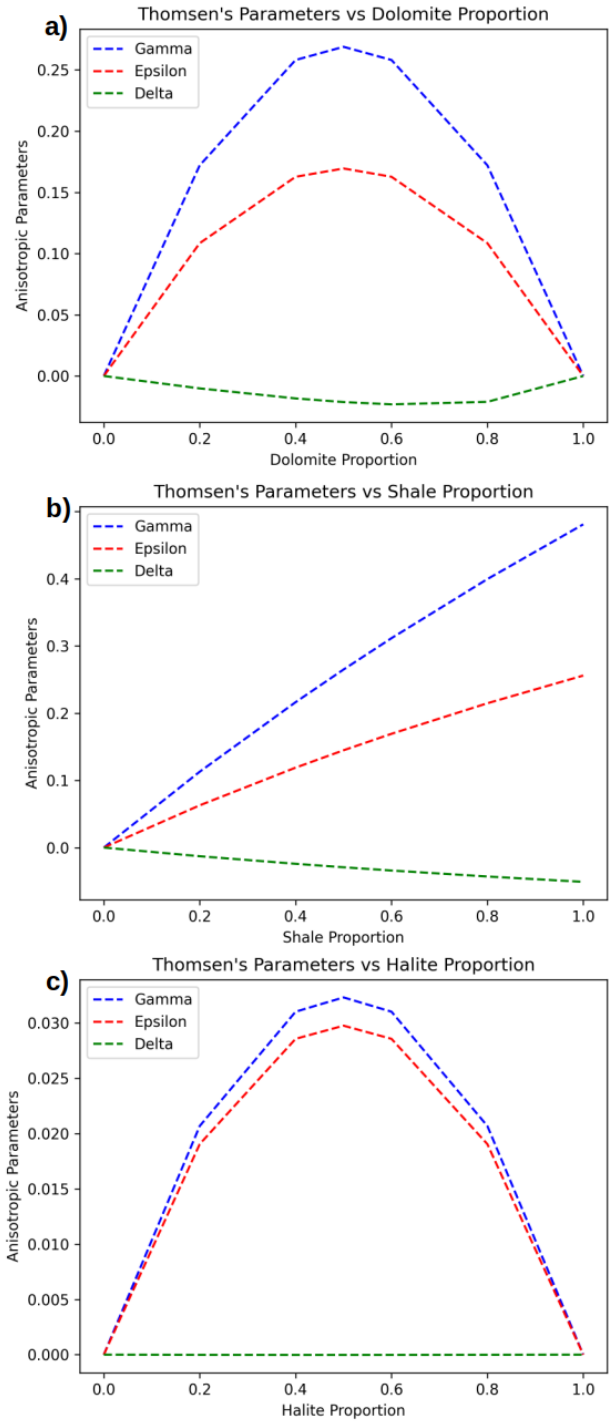

Figure 2: Effective parameters estimated for the following intercalations: a) dolomite and argillite; b) shale and sandstone; c) halite and HVS intercalation.

Forward seismic modeling

The first group of seismograms presented corresponds to the modeling carried out simulating intercalations between argillite and dolomite (Figure 3), with layer thicknesses varying between 2.5 meters and 20 meters. Initially, it is possible to indicate through visual analysis a great similarity between the seismograms representing the thicknesses of 2.5 and 5 meters.

The strongest amplitude observed corresponds to the arrival of the compressional wave, with its maximum at the point where the source-receiver distance is smaller, following to the most distant offset positions, where the amplitudes decrease. In addition to the recording of the qP wave, the arrival of the shear wave is also observed, with an opening angle according to its lower speed. Having an amplitude that allows its easy identification, the qS wave suggests that the anisotropy of the medium tends to have medium to high degree.

The seismogram corresponding to the 7.5-meter layers presents great similarity with those previously seen, especially with respect to the qP wave. However, there seems to be a relative decrease in the amplitude of the shear wave recording, as well the presence of a very faint feature next to it.

The last three seismograms, corresponding to the models with thicknesses of 10, 15 and 20 meters, have similar characteristics and can thus be grouped for analysis. Although the kinematic component of the primary wave initially corresponds to the characteristics observed in the previous examples, being possible to indicate here an increasing degree of influence of the reverberations and in the case of 20 meters, the shorter offsets present alterations due to the interaction between them and the qP wave.

The resurgence of reverberations in these three seismograms especially affects the recording of the shear wave, which can no longer be correctly identified. It is thus observed that even in a context conducive to the propagation of secondary waves, the succession of thicker layers can lead to interferences that impair the acquisition/visualization of these data.

Next, the seismograms corresponding to the sandstone and shale models are presented (Figure 4), which show a behavior similar to that observed in the seismograms for the dolomite/argillite case. Thus, for thicknesses of 2.5 and 5 meters, we have well-delineated records of compressional and shear waves, with the amplitude of the wave qP decreasing as the distance increases, while the clear character of the wave qS suggests a degree of anisotropy between medium and high.

The example of modeling with a thickness of 7.5 meters introduces the same point previously observed, where there is an attenuation of the shear wave and the presence, albeit with low amplitude, of features related to the reverberations. It is interesting to note the repetition of this behavior in different geological contexts, suggesting that there is some correspondence between their properties, which leads to the generation of the aforementioned reverberations from the simulation of layers with 7.5 meters.

For the 10-, 15- and 20-meter-thick models, the main characteristics of the recording corresponding to the compressional wave are maintained, with increasing interference in the qS wave and complex interaction between the reverberations. Such behavior

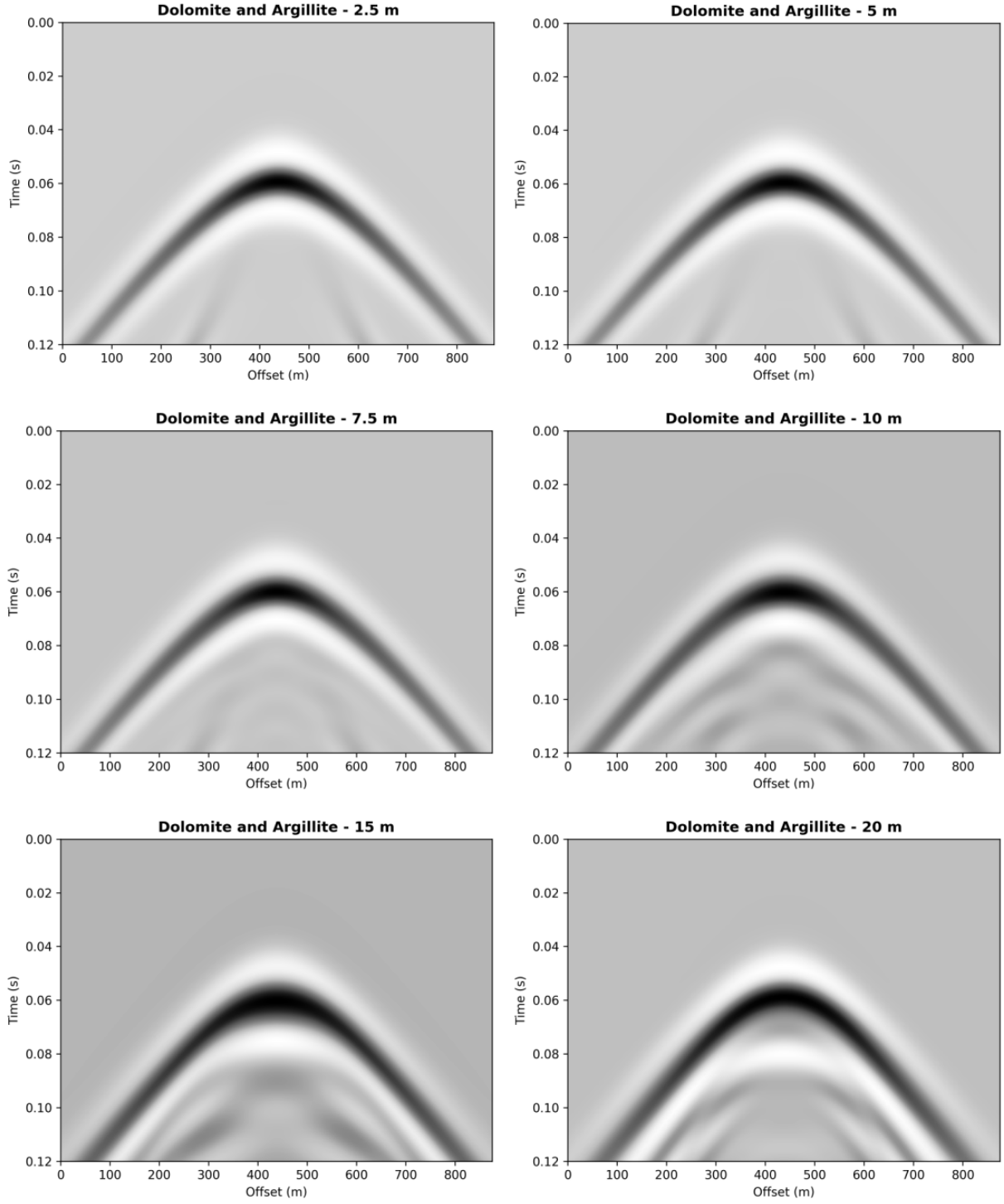

Figure 3: Seismograms for Dolomite and Argillite intercalation **with different values of layer thicknesses.**

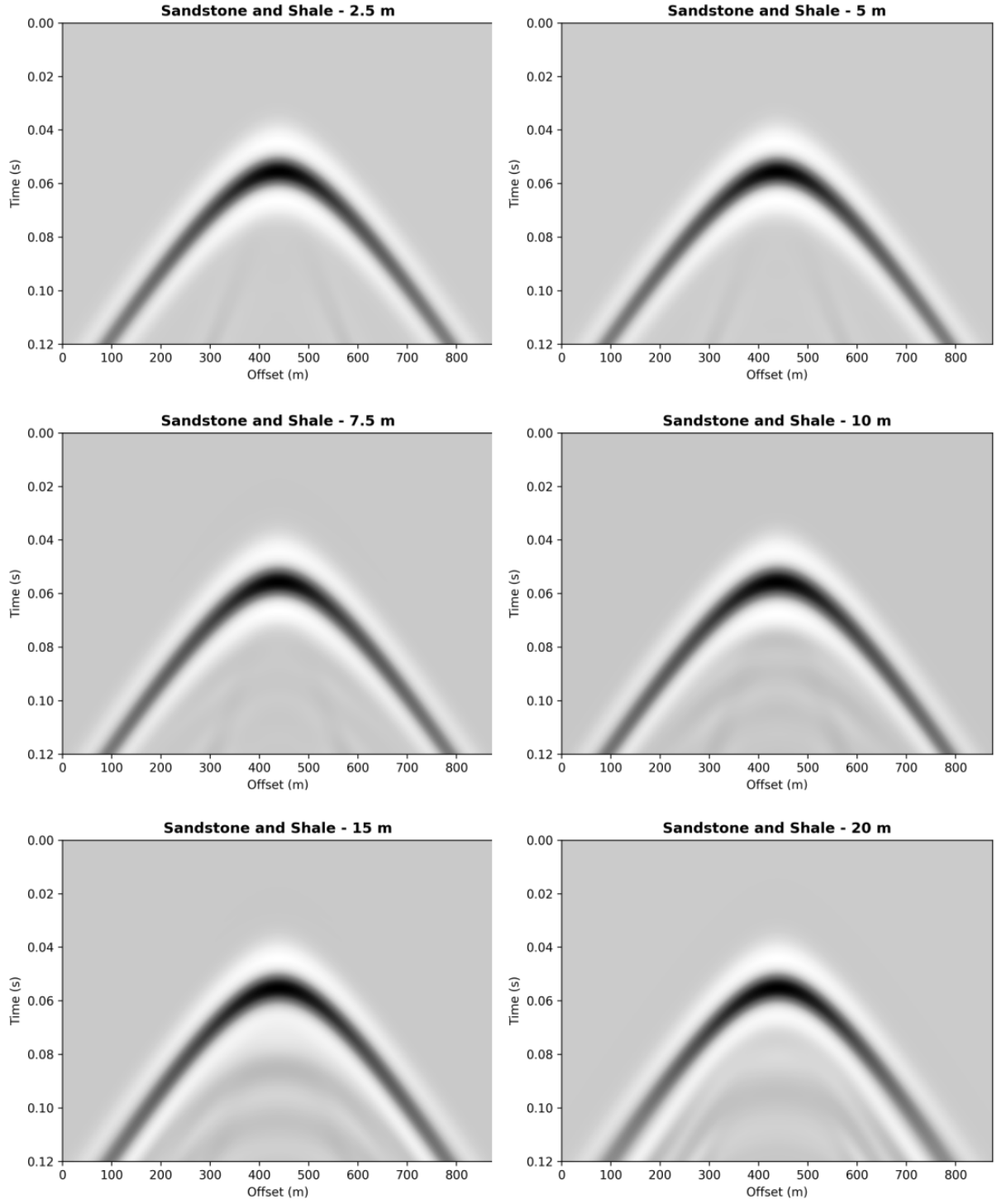

Figure 4: Seismograms for Sandstone and Shale intercalation with different values of layer thicknesses.

may suggest a limit in the ratio between wavelength and layer thickness, around which the occurrence of reverberations occurs more emphatically.

For purposes of estimating this ratio, the formulation $v = \lambda f$ can be used, considering the peak frequency of the seismic data equal to 34 Hz and the velocity of the medium equal to 3011 m/s (sandstone/shale case). This peak frequency was estimated from the analysis of the amplitude spectrum of the modeled data. In this way, we have an approximate wavelength of 88.5 meters. Assuming the case of layers with a thickness of 10 meters as the critical point, we then have the relationship $\lambda(wavelength)/thickness$ with a value close to 9.

The last sequence of modeling seismograms for stratified media corresponds to the context composed by halite and high-velocity salt (HVS), as can be seen in the Figure 5. A great similarity is observed between the representatives of the thicknesses of 2.5-, 5-, 7.5- and 10-meters-thick, with the exclusive presence of the compressional wave record. The absence of the shear wave with significant amplitude indicates that the extrinsic anisotropy generated by the intercalations has a relatively weak degree.

The presence of records corresponding to the reverberations starts occurring from the thickness of 15 meters, being visible for the analogous case of 20 meters too. Thus, for this case, we can also proceed with the estimation of the relationship between wavelength and layer thickness. Assuming the average speed of the medium equal to 4682 m/s and the frequency of 34 Hz, we have the length with a value close to 138 meters. Taking for this example the thickness of 15 meters as the starting point of highlighting reverberations, we have a relationship $\lambda/thickness$ with a value close to 9, the same as that observed for the sandstone/shale case.

After estimating the $\lambda/thickness$ relationships for the sandstone/shale and halite/HVS cases, the dolomite/argillite case can also be calculated. In this situation we have the velocity value equal to 3559 m/s and the frequency equal to 34 Hz. Thus, an estimated wavelength of 105 meters is observed. According to available data, the critical point of the reverberations is assumed for the 10-meter layers, for which the estimated relationship is approximately 10.5.

Thus, for the λ/thickness relationships, the value of 9 is obtained for the cases considering intercalations of sandstone/shale and dolomite/argillite, and the value of 10.5 for the intercalation of halite and HVS. Thus, it can be suggested that for typical cases of stratifications, ratios above 9 can configure contexts conducive to the occurrence of reverberations capable of affecting the recording of main waves, within the proposed parameterization.

The seismograms presented also serve as an indicator that the anisotropy generated by the intercalation of the layers remained in the same order of magnitude for most of the thicknesses considered, suggesting a decrease in the anisotropic effects where layer thickness is greater than 15 meters. Taking the dolomite/argillite case as an example, the λ/thickness ratios are equal to 42 and 7 for the values of 2.5 and 15 meters, thus representing a range of values where the occurrence of consistent extrinsic anisotropy can be confirmed.

Equivalent media vs Stratified media

In this section, we show the results of the modeling carried out on the stratified and equivalent media, placed side by side, allowing the assessment of similarities and differences between them. The seismograms of the intercalated media are always referring to the thickness of 2.5 meters for the layers because, as could be seen in the previous topic, thick layers give rise to reverberations, which do not exist for the homogeneous media.

Kinematic analysis

This topic begins with the presentation of the seismograms corresponding to the modeling involving halite and high-velocity salt (Figure 6a). In that image, the results obtained for the stratified and equivalent media are displayed, in addition to the presentation of a selected trace of the seismogram, allowing a more detailed observation.

For the halite/HVS case, the anisotropy generated by the intercalations in the modeling, compared to that estimated by the analytical formulations, presents values related to a weak anisotropy, close to 3%. As can be seen in the traces highlighted from the seismograms for intercalated and effective media, there is the same compressional wave recording time for both cases (0.052 s), thus showing an excellent correspondence between the propagations undertaken on the equivalent medium and on an effectively stratified medium.

Next, we present the results for the modeling using an intercalated medium composed of dolomite and argillite and for an effective medium with parameters estimated from the same lithological combination (Figure 6b). As the argillite is an isotropic lithology, the anisotropic effect is restricted to the extrinsic class.

The analysis of seismograms indicates an excellent match between the data modeled from different media (equivalent and stratified). From the selected trace, perfect conformity for the compressional wave can be observed, as well as a fully satisfactory correlation for the shear wave, with a difference of only 1 ms. Thus, there is an excellent kinematic correspondence between the results from equivalent and stratified media.

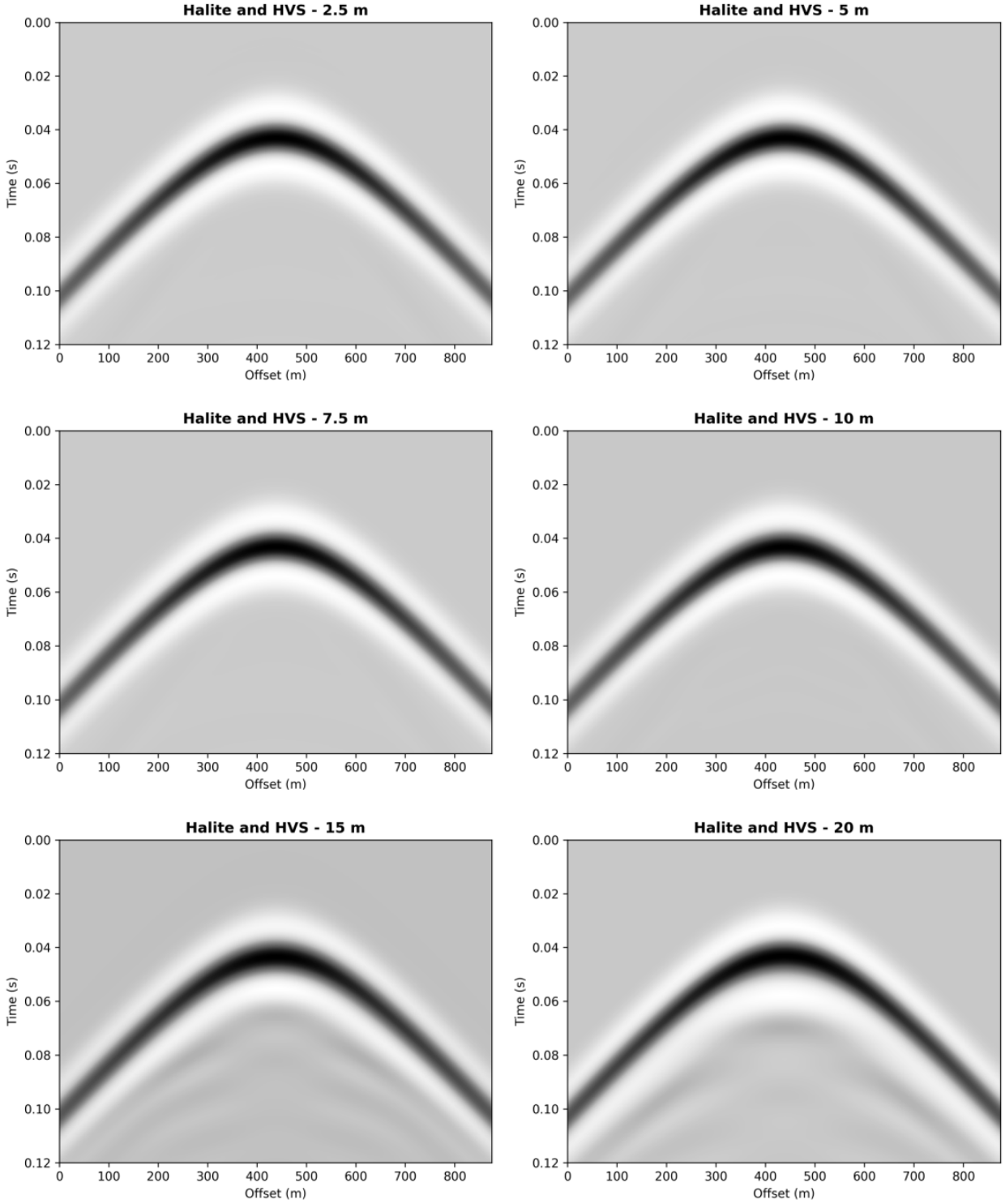

Figure 5: Seismograms for Halite and High-Velocity Salt intercalation **with different values of layer thicknesses.**

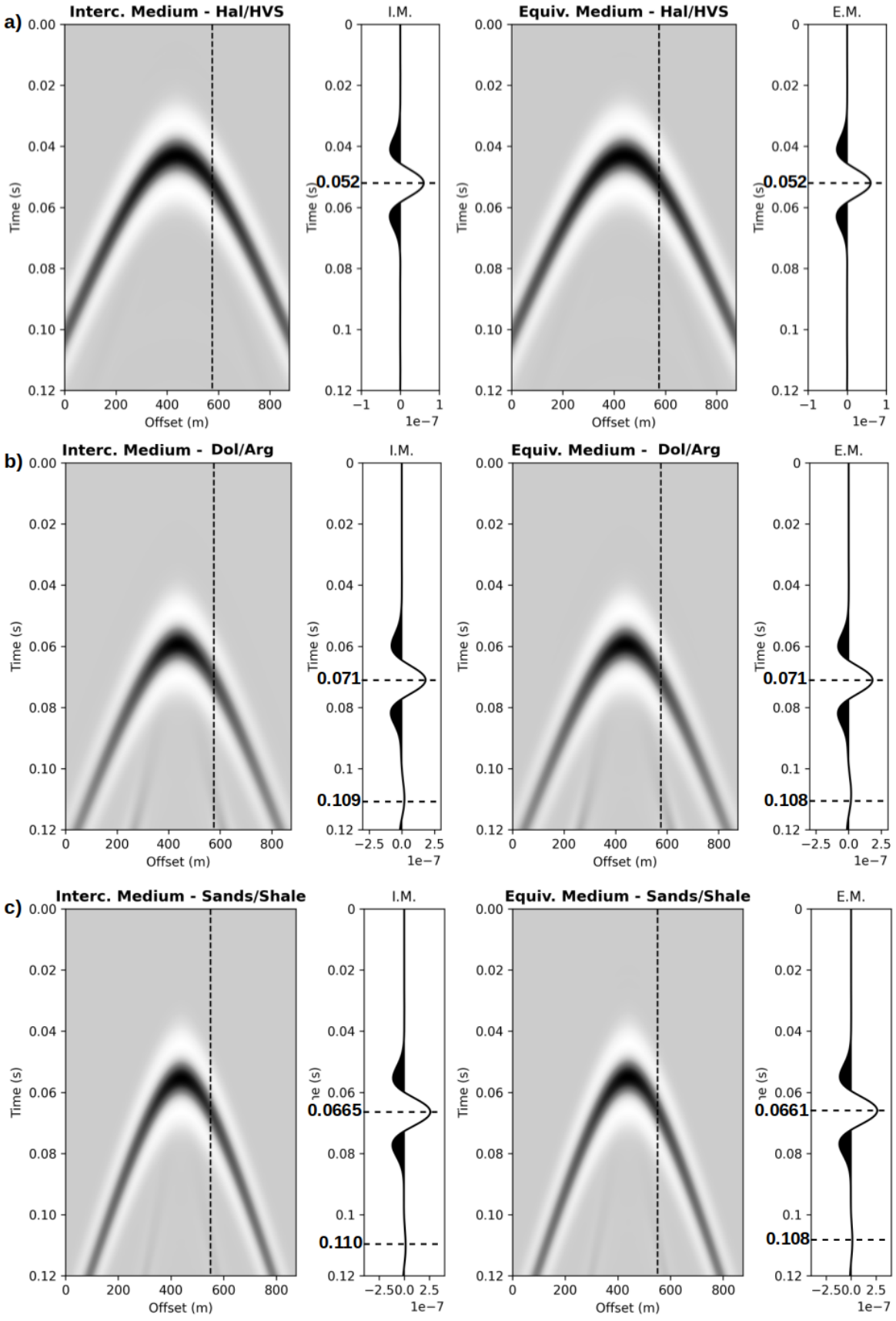

Figure 6: Seismograms for Intercalated Medium and Effective Medium: a) Halite and HVs; b) Dolomite and Argillite; c) Shale and Sandstone. The travel time values for qP and qS waves are highlighted.

The last kinematic analysis evaluates the models generated for a siliciclastic intercalation context, involving sandstone and shale (Figure 6c). For these, the largest kinematic discrepancies are observed among the cases studied, with a maximum value of 2 ms, corresponding to the difference observed for the qS wave. In the case of the qP wave, the difference in arrival time for the two models is lower, around 0.4 ms.

Since this is the only case where one of the lithologies has intrinsic anisotropy, it can be suggested that this characteristic was not incorporated by the formulations as well as the ordinary properties of velocity and density, thus generating the aforementioned discrepancies. It should be noted that the results for the equivalent medium and for the intercalated medium exhibit similar anisotropies, although not exactly the same, as observed in the other examples.

Having available seismograms for stratified media with different thicknesses and seismograms from equivalent media (EM), the maximum amplitudes of each of these were extracted so that the main features could be superimposed, as can be seen in the Figure 7. Details of the seismograms are presented next.

Beginning with the dolomite/argillite case, in Figure 8a, we observe in greater detail the difference in distances between the hyperboloids corresponding to the smallest thicknesses and those relating to the thicknesses of 15 and 20 meters. It can be observed that the green line (20 meters) has a distance from the other lines, showing that the anisotropy generated by the intercalations with this thickness seems to have been impaired for this situation. On the other hand, in the top detail (Figure 8b), where the portion of the shortest offsets is focused, we can see a perfect correspondence between the curves of the effective medium and the 2.5- and 5-meter thick curves, indicating that in kinematic terms, we have a good representation of these stratified media by an equivalent medium.

In Figure 8c we present the hyperboloids for the sandstone/shale with different thickness. These hyperboloids are very close which suggest the anisotropy remained stable for all scenarios. The upper detail in Figure 8d shows a grouping between the curves of effective media and stratified one for thicknesses of 15 and 20 meters. Considering that such thicknesses are at the limit of extrinsic anisotropy occurrence, we have that the effective media for this case does not have estimates as reliable as those obtained for the dolomite/argillite case.

For the intercalation between halite and high-speed salt, we have the case where the curves are closer to each other (Figs. 8e and 8f). That behavior is directly related to the weak anisotropy generated and indicates that the kinematic differences for the distincts thicknesses are very small, in contrast to the behavior observed for the other scenarios.

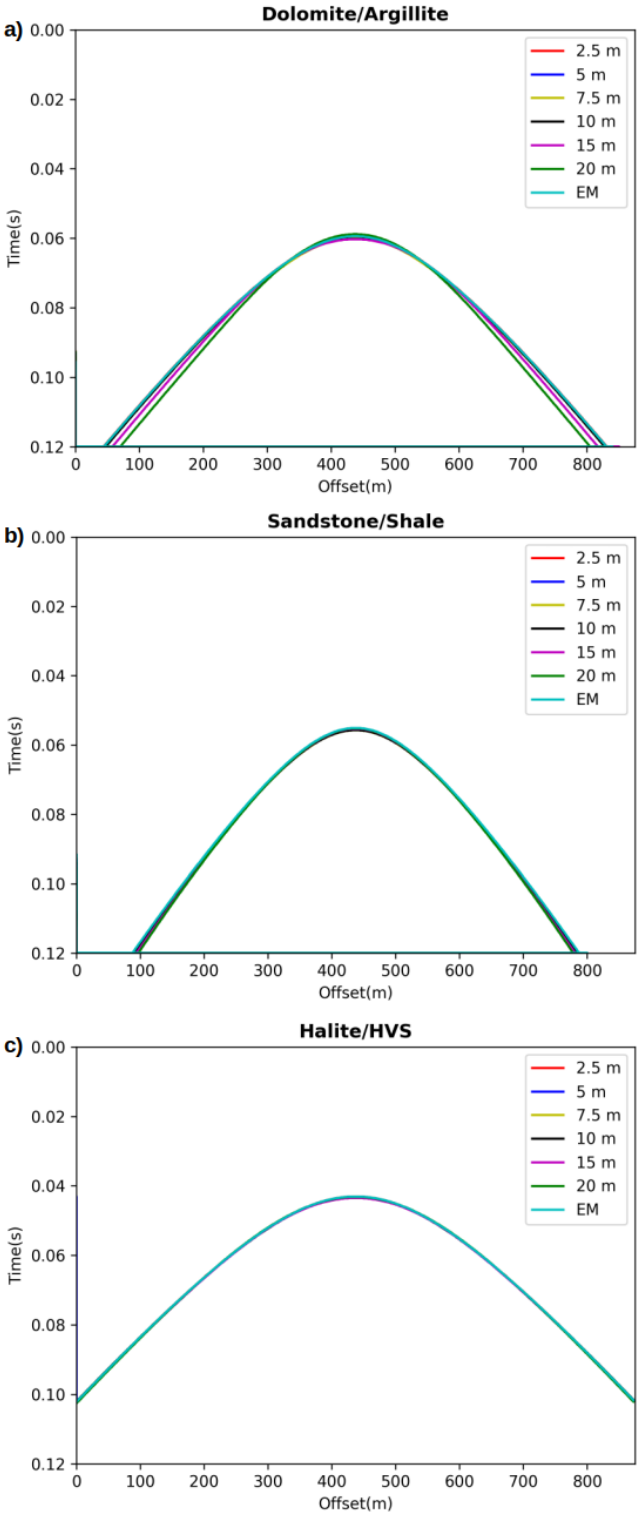

Figure 7: Superposition of the maximum amplitudes extracted from the seismograms for kinematic analysis: a) dolomite/argillite; b) sandstone/shale; c) halite/high-velocity salt. **The colors represent different layer thicknesses.**

By superimposing the hyperboloids extracted from the seismograms, it is possible to detail the wavelength-to-layer-thickness ratios from which there is no consistent generation of anisotropy. For the two cases where the curves diverge (Figs. 8a and 8c), the limit is observed for layers with thicknesses of 15 meters. Thus, in the dolomite/argillite context the long-wave anisotropy is generated in ratios greater than 7, while in the sandstone/shale case, in ratios greater than 6.

Amplitude analysis

The comparison of the amplitudes obtained for the modeling carried out with layers of different thicknesses, as well as for the equivalent medium, is presented in the figures of this section. For the detailed analysis, traces selected from seismograms of each model were used, corresponding to the distances of 0, 82.5 and 207.5 meters. These offsets seek to represent, within the scale of the model, variations in amplitude depending on the distance between source and receivers, providing insights for analyzes of this nature.

Initially, Figure 9 shows the seismograms corresponding to the modeling for intercalated media (considering thicknesses of 2.5 meters for the layers) and for the effective one for the three geological contexts evaluated, along with the differences between them. This difference corresponds to the subtraction of one seismogram by the other, so that in case of perfect kinematic and dynamic correspondence, the result would be a matrix of zeros.

In Figure 9a we have the results obtained for the intercalation between halite and high-speed salt, where the difference panel indicates an excellent correspondence between the two seismograms on the left, Figure 9b presents the results for the intercalation between dolomite and argillite, where the difference panel has values other than zero, although it is a relatively small difference between the seismograms.

Finally, in Figure 9c, corresponding to the sandstone/shale case, we have the difference of the most prominent features among the evaluated contexts, although composed of relatively low values. These values results from the kinematic difference between the modeling done for interleaved and equivalent media; although small, they imply that the subtraction of the seismograms ends up comparing points that are not exactly correspondent. It can thus be suggested, similarly to the kinematic analysis, that this case is the most complex context for these comparisons, due to the presence of an intrinsically anisotropic lithology.

In Table 4, the amplitudes collected from the seismograms generated with different thicknesses in the Halite-HVS context are presented, considering traces with different distances. It can be observed that the values remain relatively stable up to a thickness of 10 meters, with a sharp decrease from this point onwards. As observed in the previous topic, where the reverberations were highlighted in the seismograms, we observe a reduction of the registered amplitudes because part of the energy is dispersed in the referred events.

Table 4: Comparison of maximum amplitudes for layers with different thicknesses and Equivalent Medium (Halite/HVS).

Layers	0 m	82.5 m	207.5 m
2.5 m	6.94	6.52	5.36
5 m	6.94	6.51	5.36
7.5 m	6.95	6.49	5.35
10 m	6.91	6.38	5.28
15 m	6.44	5.97	4.91
20 m	5.83	5.61	4.74
EM	6.94	6.52	5.36

The amplitudes observed for the equivalent medium correspond exactly to those observed for the stratified media with thinner thicknesses, differing only from the point where the reverberations act more emphatically. Such correspondence suggests that the effective medium can be configured as an excellent representation of an intercalated medium when this is formed by thinner layers.

The Table 5 presents the values of the amplitudes for the dolomite/argillite case. We observe a relatively weak change in the values from thickness of 7.5 meters, as well as a sudden variation of the amplitudes in thickness of 10 meters. As in the previous example, the disturbance in amplitude is correlated with the prominent presence of reverberations. The values read for the effective medium present excellent correspondence when compared to the numbers obtained for the thinner layers, thus confirming the validity of its representativeness for contexts of this nature.

The last amplitude analysis presents the data referring to the modeling for siliciclastic intercalations. The observation of the amplitudes arranged in the Table 6 reveals that this context is the one with the smallest reduction in the values collected, suggesting that the loss of energy for the reverberations occurred in a weaker way. This indication may be correlated to the relatively small contrast between the vertical velocities of the sandstone and the shale, thus suggesting that situations with greater discrepancies between properties are more susceptible to this type of effect.

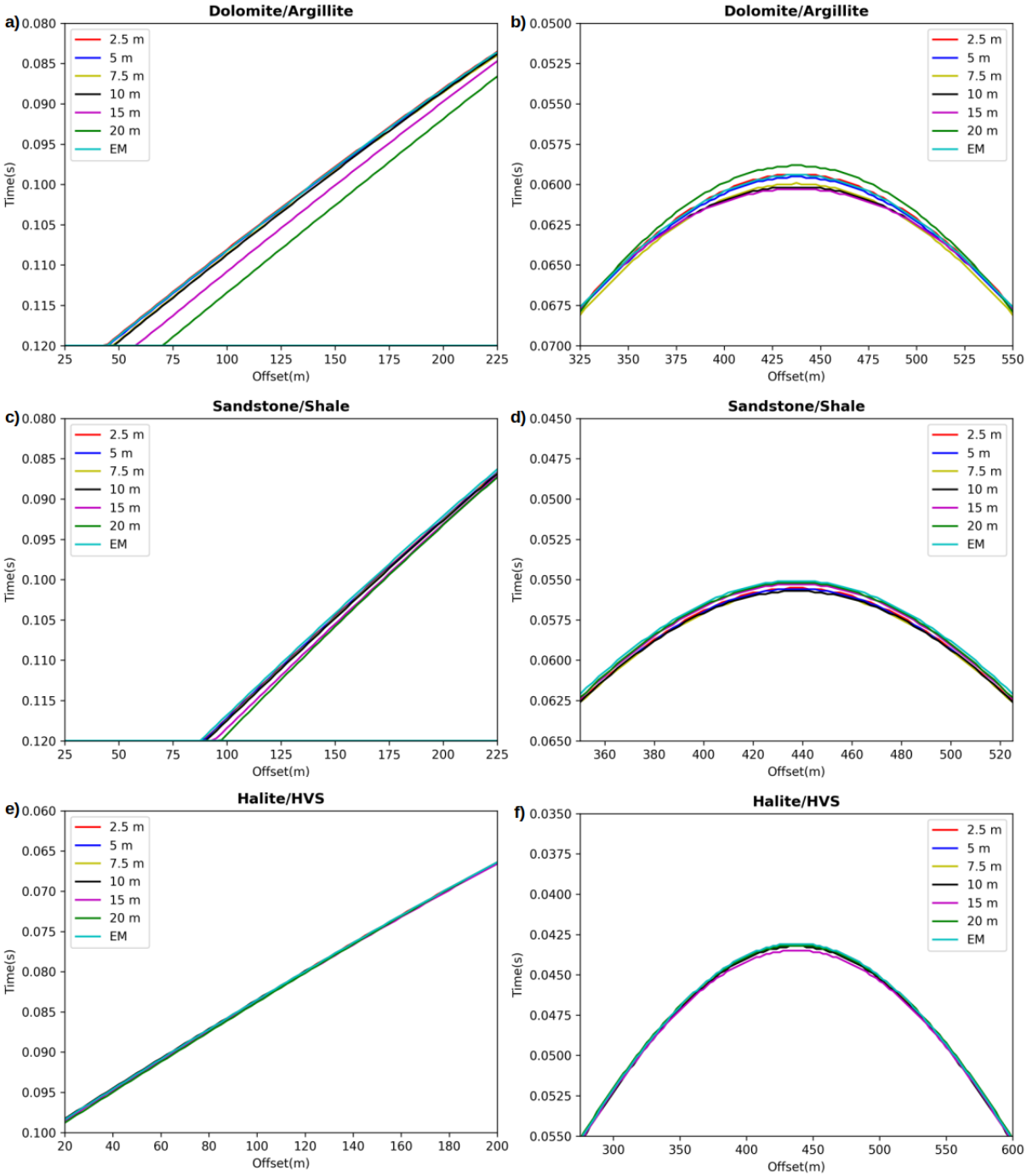

Figure 8: Side and top details of the maximum amplitude overlap for kinematic analysis: a) dolomite/argillite; b)sandstone/shale; c) halite/HVS.

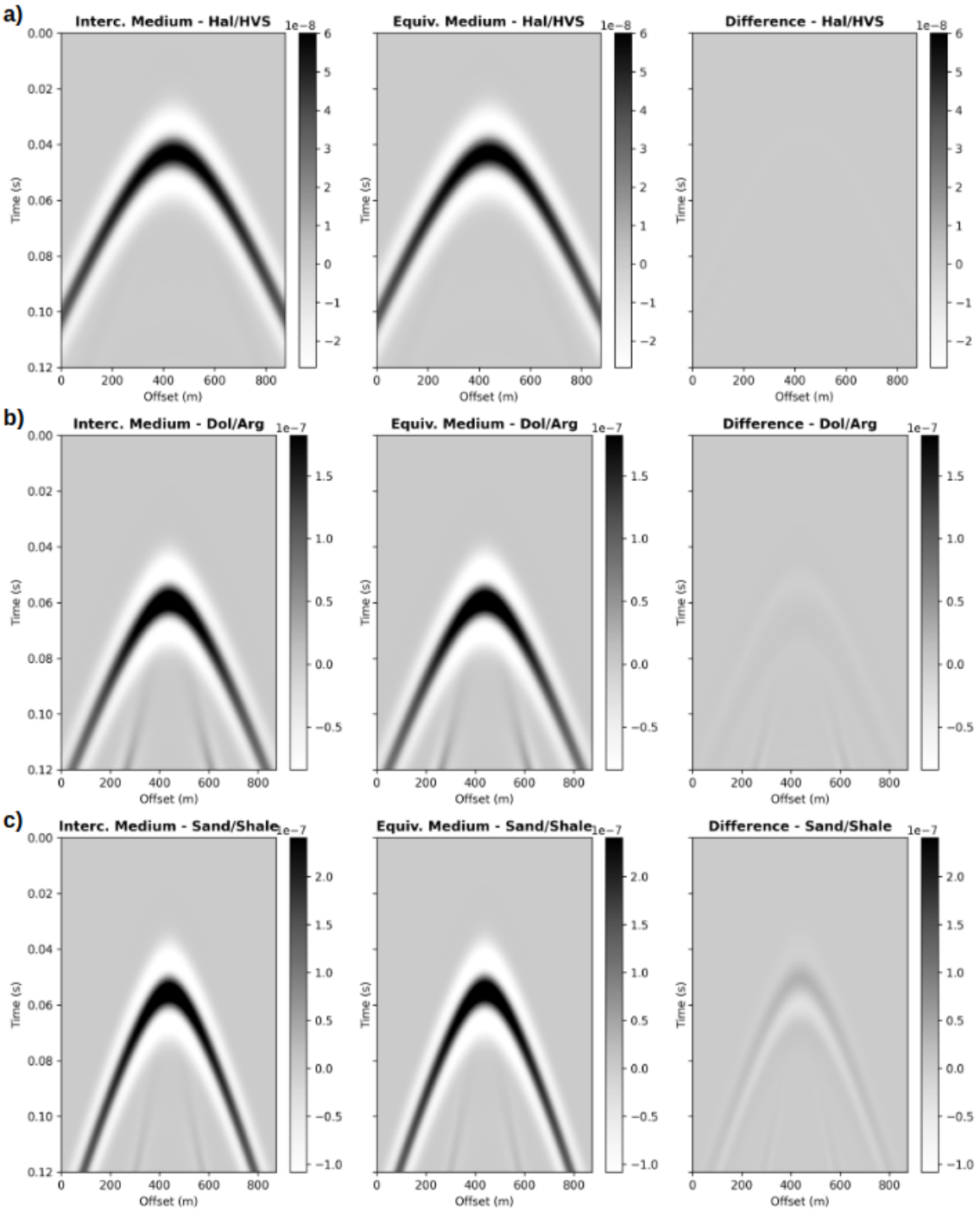

Figure 9: Seismograms of Intercalated Medium, Effective Medium and Difference between them: a) Halite and HVS; b) Dolomite and Argillite; c) Sandstone and Shale. **Normalized amplitude scale for comparison.**

Table 5: Comparison of maximum amplitudes for layers with different thicknesses and Equivalent Medium (Dolomite/Argillite).

Layers	0 m	82. m	207.5 m
2.5 m	2.72	2.21	1.45
5 m	2.73	2.19	1.46
7.5 m	2.70	2.08	1.44
10 m	2.46	1.88	1.34
15 m	1.73	1.57	1.23
20 m	1.54	1.47	1.10
ME	2.71	2.22	1.45

The values corresponding to the equivalent medium again present an excellent correlation with those observed for the smallest thicknesses, proving that there is an excellent correspondence between the effective medium and the stratified medium, when the second is formed by relatively thin layers. Such observation can serve as a guide for situations where it is intended to simplify the representation of a heterogeneous medium by a homogeneous medium, indicating when the amplitude may or may not present a good correspondence.

Table 6: Comparison of maximum amplitudes for layers with different thicknesses and Equivalent Medium (Sandstone/Shale).

Layers	0 m	82.5 m	207.5 m
2.5 m	3.58	2.88	1.99
5 m	3.58	2.87	2.0
7.5 m	3.54	2.82	2.0
10 m	3.35	2.75	1.97
15 m	3.19	2.68	1.89
20 m	3.28	2.74	1.78
ME	3.58	2.88	1.99

Extrinsic and intrinsic anisotropies

From the experiments above, it is remarkable that anisotropy may be composed of the intrinsic elements of the lithologies present in a sedimentary interval, as well as by the thin intercalation of layers with different properties (extrinsic anisotropy). Next, the results of two seismic modeling are presented, undertaken with the objective of verifying the participation of different anisotropies (intrinsic and extrinsic) in the generation of anisotropy in a medium.

The models were generated from the sandstone and shale parameters presented by Sondergeld and Rai (2011), as indicated in Table 2. Initially, we have on the upper part of Figure 10 the representation of the pressure field obtained from the seismic modeling for the stratified medium of sandstones and shales, where both lithologies are assumed to be isotropic.

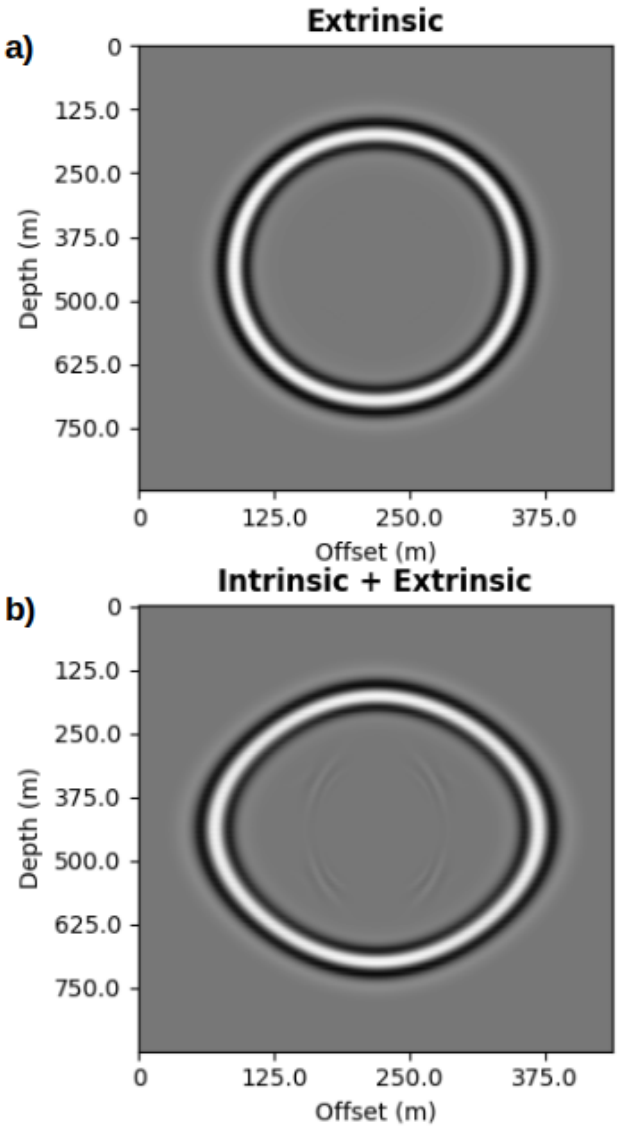

Figure 10: Pressure fields for modeling with: a) sandstone and isotropic shale; b) sandstone and anisotropic shale.

Figure 10a shows a snapshot of the propagation in such media, where the wavefront shape is almost circular,thus suggesting that the velocity contrast between the sandstone and the shale, equal to 110 m/s, is unable to generate a significant anisotropic effect, preliminarily indicating that the occurrence of extrinsic anisotropy depends on greater differences between the properties of the lithologies considered.

Figure 10b shows the snapshot of the pressure field, but differing from Figure 10a, in this experiment there is the intercalation of sandstone and shale, where we consider the anisotropy of the shale. As can be seen in the figure indicated, the pressure field has the shape of a deformed ellipse, as expected for an anisotropic medium. Also, it is possible to observe the q-S wave field, not visible in the previous figure. This experiment show how important is the effect of intrinsic anisotropy despite the small elastic contrast between the considered lithologies.

Complementing the observations presented above, Figure 11 shows the seismograms corresponding to the two modeling carried out for this stage. On the upper part of the figure, the case where the sandstone and the shale are considered as isotropic is presented, and below, the result obtained when the anisotropy of the shale was considered is displayed. The first point to be highlighted is the difference between the openings of the hyperboloids that is greater for the case composed of intrinsic anisotropy plus extrinsic anisotropy. Similar to what was observed for the pressure fields, the presence of the record corresponding to the shear wave in the figure on the right is an important indicator of the occurrence of a prominent anisotropic effect.

This set of results confirms a good correspondence between the values estimated from the analytical formulations and the values obtained from the modeling experiments, so that the resulting anisotropy can be indicated for the modeling where the shale was considered as isotropic (Figure 12).

In the sandstone/shale example disregarding shale anisotropy, epsilon is equal to 0.005 for a 50% proportion of each lithology, which configures an extremely weak anisotropy. Such experiment allows understanding the circular feature observed in Figure 10, showing that the anisotropy generated by the intercalation of the layers is really very subtle.

These modelings indicate that, for the analyzed case, the main anisotropic element corresponds to the intrinsic anisotropy of the shale, that is, the effect generated by the alignment of the minerals of this lithology predominates over the differences in vertical velocity indicated for the two rocks considered.

The results presented above show that the occurrence of significant extrinsic anisotropy depends on considerable velocity contrasts, since small differences generate a relatively homogeneous medium with respect to the passage of a seismic wave.

For the modeled evaporitic case, there is a contrast of 551 m/s between the velocities of the two lithologies, and the highest anisotropy value can be observed at the point where there is a proportion of 50% for each rock. The value of ϵ is equal to approximately 0.03, thus corresponding to a weak anisotropy. As for the intercalation between dolomite and argillite, the velocity contrast is 2300 m/s, with ϵ reaching a maximum value close to 0.17.

The experiments show that intercalation of two isotropic materials causes the highest anisotropy whenever there is a 50% proportion of each material. The anisotropy intensity is proportional to the elastic contrast between the two materials. Furthermore, the experiments show that higher anisotropic effects occur whenever there is at least one anisotropic material composing the intercalation of two lithologies and their intensity depends on the proportion of the anisotropic material.

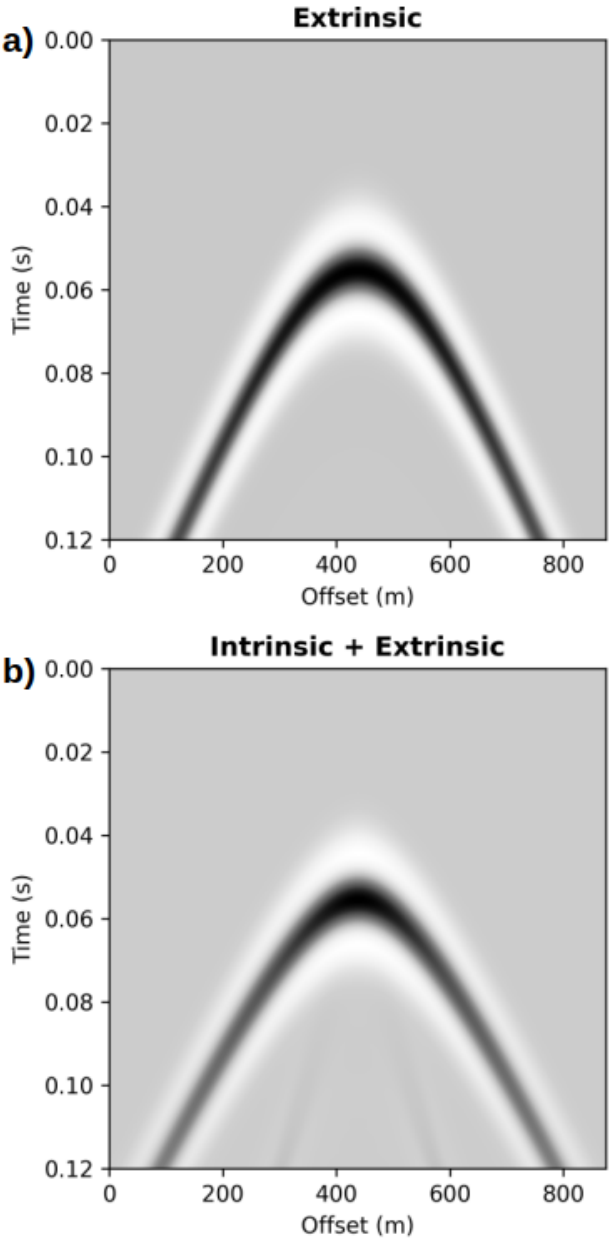

Figure 11: Seismograms for modeling with: a) sandstone and isotropic shale; b) sandstone and anisotropic shale.

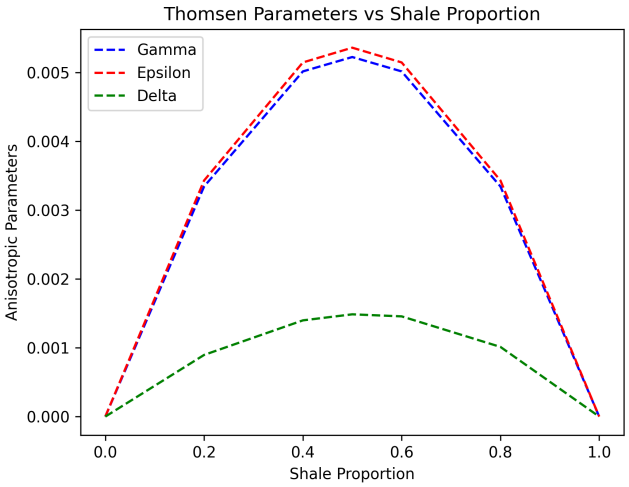

Figure 12: Anisotropic parameters estimated for intercalations of sandstone and isotropic shale.

DISCUSSIONS

The estimates obtained for the dolomite and argillite cases indicated the highest extrinsic anisotropy among all the analyzed contexts, with the parameter ϵ reaching the value of 0.17. Such result shows that intercalations of this nature, with great contrast between the elastic properties, must be diligently analyzed, since they can significantly influence the velocity models.

For the siliciclastic intercalation case, we have a different behaviour, resulting from anisotropic shale, where it is possible to observe that the presence of clay sheets in the proportion of 20% inside the sedimentary package is capable of generating weak anisotropy, not negligible.

As for the intercalation between halite and high-velocity salt, the behavior is close to that observed for the intercalation between dolomite and claystone, although it has a much lower maximum anisotropy value. Thus, for lithologies with these elastic properties, it can be indicated that the presence of rare HVS layers does not result in significant anisotropy.

The different geological contexts evaluated allowed the observation of how the contrasts between the compressional velocities of the lithologies influence the generation of anisotropy, thus covering the situations most frequently found in the sedimentary basins. For a contrast of 110 m/s, the estimated value of ϵ was equal to 0.005; for a contrast of 551 m/s, ϵ was estimated to be 0.03; and, finally, for a contrast of 2300 m/s, ϵ corresponds to 0.17.

Comparisons made between the equivalent and stratified media models show an excellent kinematic and dynamic correspondence for situations where the layers are less than 5-meters thick. For greater thicknesses, the reverberations that occur in the intercalated media start to affect the amplitudes significantly, decreasing the correspondence between the different media.

Thus, modeling of stratified media showed that wavelength to layer thickness ratios less than 6 are not conducive to the generation of consistent extrinsic anisotropy, in addition to being associated with the occurrence of expressive reverberations. These observations serve as an important reference for situations where the aim is to simplify an intercalated medium, representing it through a homogeneous equivalent medium.

The lithological combinations presented seek to expand the analysis carried out by Carcione et al. (1991), who present similar values for the relationship between wavelength and thickness, highlighting the interaction between sandstone and carbonate. Amplitude analyzes also constitute a new element, showing that internal reverberations can affect the seismic record.

Finally, in the analysis presented about the contributions of intrinsic and extrinsic anisotropy in an intercalation composed by sandstones and shales, we showed that it is possible to indicate that the former is the main responsible for the effective anisotropy of the package. This highlights the importance of recognizing the intrinsic properties of each lithology for analyzes of this nature, reinforcing the importance of anisotropic characterization of shales, since they constitute a prominent lithology within this theme.

CONCLUSIONS

By combining anisotropy estimates obtained from analytical formulations and from numerical modeling of homogeneous, anisotropic and stratified media, we observed good correspondence of the results. Also, it is indicated that for wavelength versus thickness ratios with values greater than 6, there is consistent generation of long-wave anisotropy.

The good adherence obtained within the proposed limit serves as an important guide for the construction of velocity models, especially for contexts of stratified media composed by thin layers, which can be adequately represented by homogeneous features, maintaining the coherence of kinematic and dynamic properties.

The experiment carried out in order to determine the contribution of the intrinsic anisotropy and the long-wave anisotropy allows us to indicate that, for the analyzed context, the second has a greater influence on the magnitude of the general anisotropy, confirming the importance of the correct configuration of the shale layers in velocity model building.

The analysis of different geological contexts from analytical estimates and seismic modeling proved to be an effective methodology to understand how the different contrasts between elastic properties act in the formation of anisotropy, adding information about how each lithology can be treated in seismic imaging process.

REFERENCES

Aniwetalu, E., E. Anakwuba, and J. Ilechukwu, 2021, Velocity anisotropy and trend in Niger Delta, Nigeria: Journal of Petroleum Exploration and Production, **11**, 1667–1678, doi: 10.1007/s13202-021-01136-y.

Backus, G. E., 1962, Long-wave elastic anisotropy produced by horizontal layering: Journal of Geophysical Research, **67**, 4427–4440, doi: 10.1029/JZ067i011p04427.

Carcione, J. M., D. Kosloff, and A. Behle, 1991, Long-wave anisotropy in stratified media: A numerical test: Geophysics, **56**, 245–254, doi: 10.1190/1.1443037.

Dewhurst, D. N., and A. F. Siggin, 2006, Impact of fabric, microcracks and stress field on shale anisotropy: Geophysical Journal International, **165**, 135–148, doi: 10.1111/j.1365-246X.2006.02834.x.

Kumar, D., 2013, Applying Backus averaging for deriving seismic anisotropy of a long-wavelength equivalent medium from well-log data: Journal of Geophysics and Engineering, **10**, 055001, doi: 10.1088/1742-2132/10/5/055001.

Lupinacci, W. M., L. d. M. S. Gomes, D. J. A. Ferreira, R. Bijani, and A. F. M. Freire, 2020, An integrated approach for carbonate reservoir characterization: A case study from the Linguado Field, Campos Basin: Brazilian Journal of Geology, **50**, 1–12, doi: 10.1590/2317-4889202020190103.

Martins, E. O., 2003, Modelagem sísmica em meios complexos: Master's thesis, Universidade Federal do Rio de Janeiro (UFRJ), Rio de Janeiro, Brazil.

Maul, A. R., M. A. C. Santos, C. G. Silva, L. M. T. d. Silva, M. d. L. González Farias, J. S. d. Fonseca, R. d. M. Dias, J. B. T. Boechat, F. A. d. S. Borges, L. F. Fernandes, T. M. Yamamoto, and R. L. B. Pontes, 2019, Improving pre-salt reservoirs seismic images when considering the stratified evaporites insertion in the initial model for the velocity updating processes prior to the seismic migration: Brazilian Journal of Geophysics, **37**, 235–248, doi: 10.22564/rbgf.v37i3.2004, issn = 0102-261X.

Mavko, G., T. Mukerji, and J. Dvorkin, 2009, *in* The Rock Physics Handbook: Tools for Seismic Analysis of Porous Media: Cambridge University Press, 147–153.

McCollum, B., and F. A. Snell, 1932, Asymmetry of sound velocity in stratified formations: Physics, **2**, 174–185.

Melia, P. J., and R. L. Carlson, 1984, An experimental test of P-wave anisotropy in stratified media: Geophysics, **49**, 374–378, doi: 10.1190/1.1441673.

Okorie, I. P. C., J. O. Ebeniro, and C. N. Ehirim, 2016, Anisotropy and empirical relations for the estimation of anisotropy parameters in Niger Delta Depobelts: International Journal of Geosciences, **7**, 345–352, doi: 10.4236/ijg.2016.73027.

Singh, A., and A. Sircar, 2014, Sources and measurement of velocity anisotropy of Cambay Shale, Cambay Basin, India: IJLTEMAS, **3**, 169–179.

Sondergeld, C. H., and C. S. Rai, 2011, Elastic anisotropy of shales: The Leading Edge, **30**, 324–331, doi: 10.1190/1.3567264.

Teixeira, B., 2021, Caracterização dos reservatórios turbidíticos da Porção Centro-Norte do Novo Campo de Jubarte, Bacia de Campos, baseada na interpretação integrada de dados de rocha, perfis de poço e sísmica 3D: Master's thesis, Universidade Federal Fluminense (UFF), Rio de Janeiro, Brazil.

Thomsen, L., 1986, Weak elastic anisotropy: Geophysics, **51**, 1954–1966, doi: 10.1190/1.1442051.

da Silva, G.H.T.: code development, methodology, original draft - writing, review & editing; **Santos, L.A.:** code development, methodology, review & editing; **Santos, M.A.C.:** methodology, review & editing.

Received on July 31, 2023 / Accepted on November 6, 2023